Supporting Information

Controllable synthesis of electric double layer capacitance and pseudocapacitance coupled porous carbon cathode material for zinc-ion hybrid capacitors

Xiaoyi Pan [a #], Qian Li [a #], Tongde Wang [b,] Tie Shu [c] Yousheng Tao [a*]

[a] College of Materials Science and Engineering, Sichuan University, Chengdu, 610065, People's Republic of China

[b] Shanghai Key Laboratory of Special Artificial Microstructure Materials and Technology, School of Physics Science and Engineering, Tongji University, Shanghai 200092, China.

[c] Multi-scale Porous Materials Center, Institute of Advanced Interdisciplinary Studies, & School of Chemistry and Chemical Engineering, Chongqing University, Chongqing 400044, People's Republic of China

*Corresponding author. E-mails: taoys@scu.edu.cn (Yousheng Tao)

 # Xiaoyi Pan and Qian Li contributed equally to this manuscript.

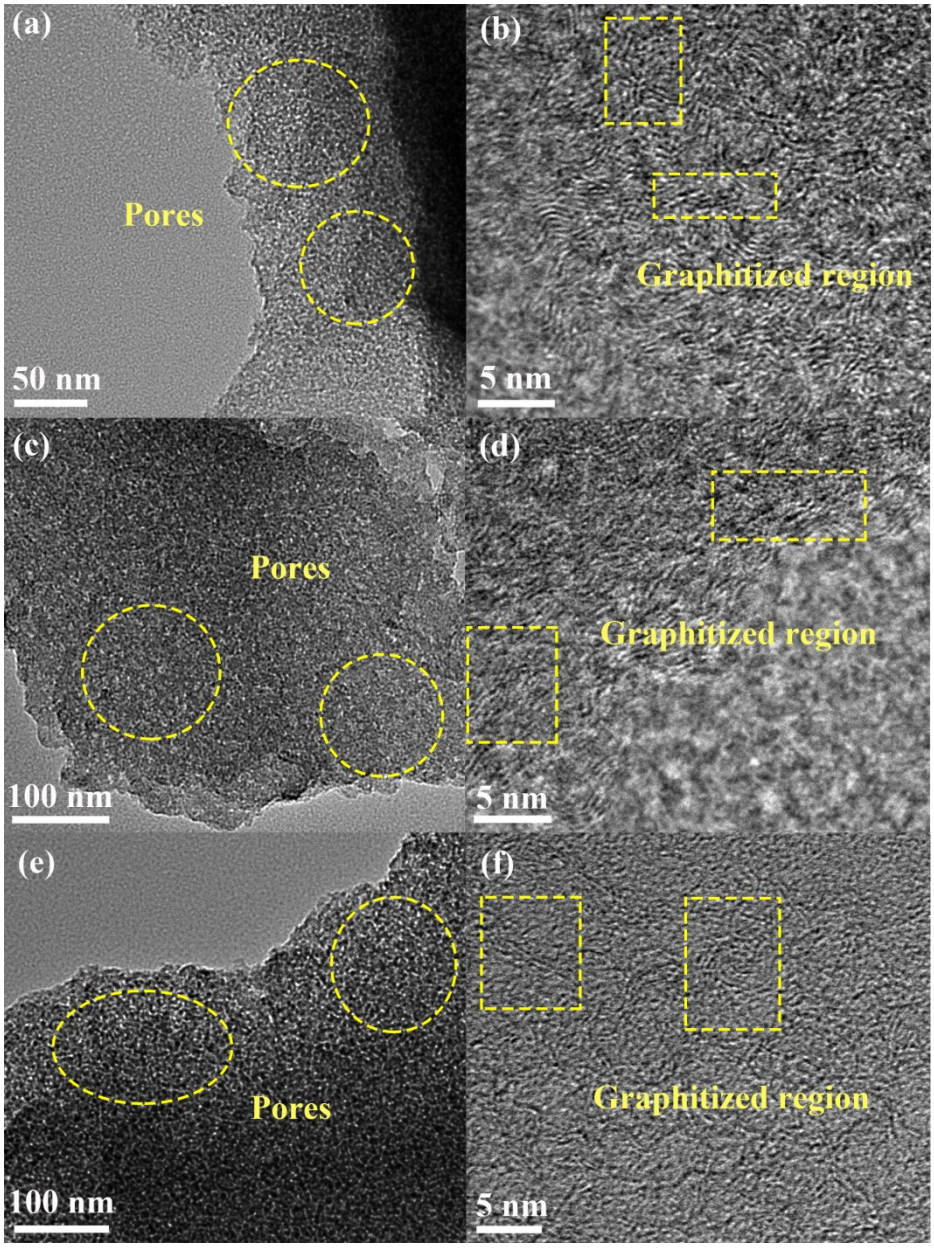

Figure S1 TEM image of (a,b) Pure, (c,d) SA-2, (e,f) SA-4.

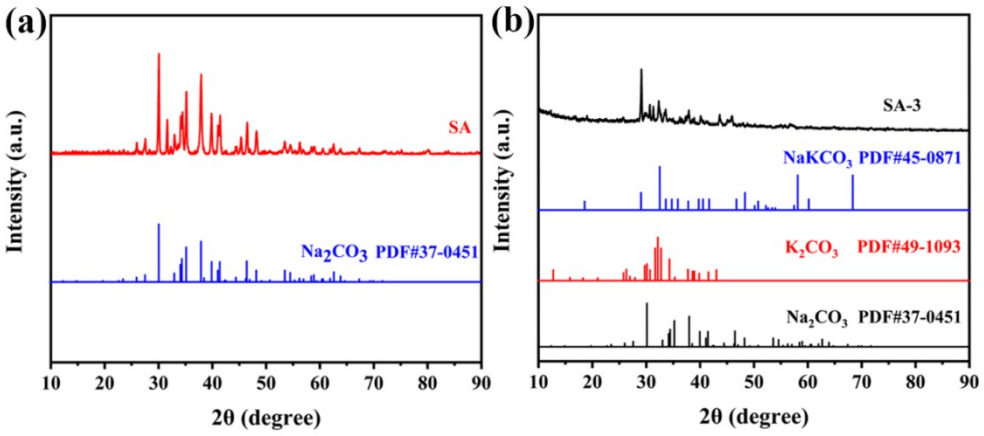

Figure S2 XRD before cleaning

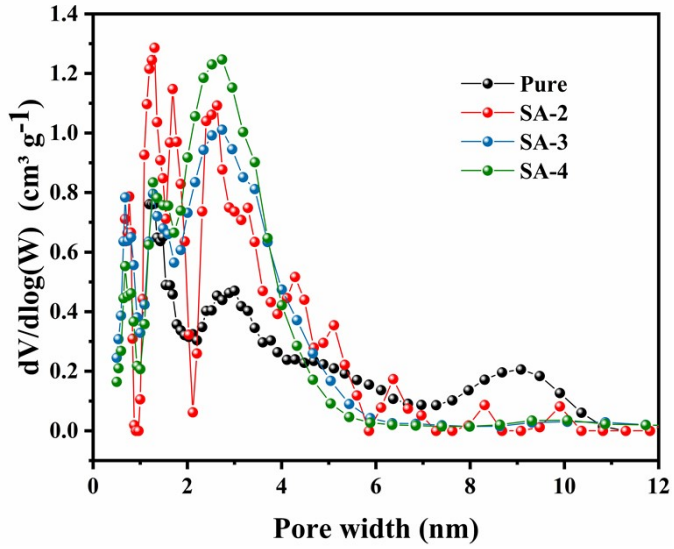

Figure S3 pore size distributions of Pure, SA-2, SA-3 and SA-4

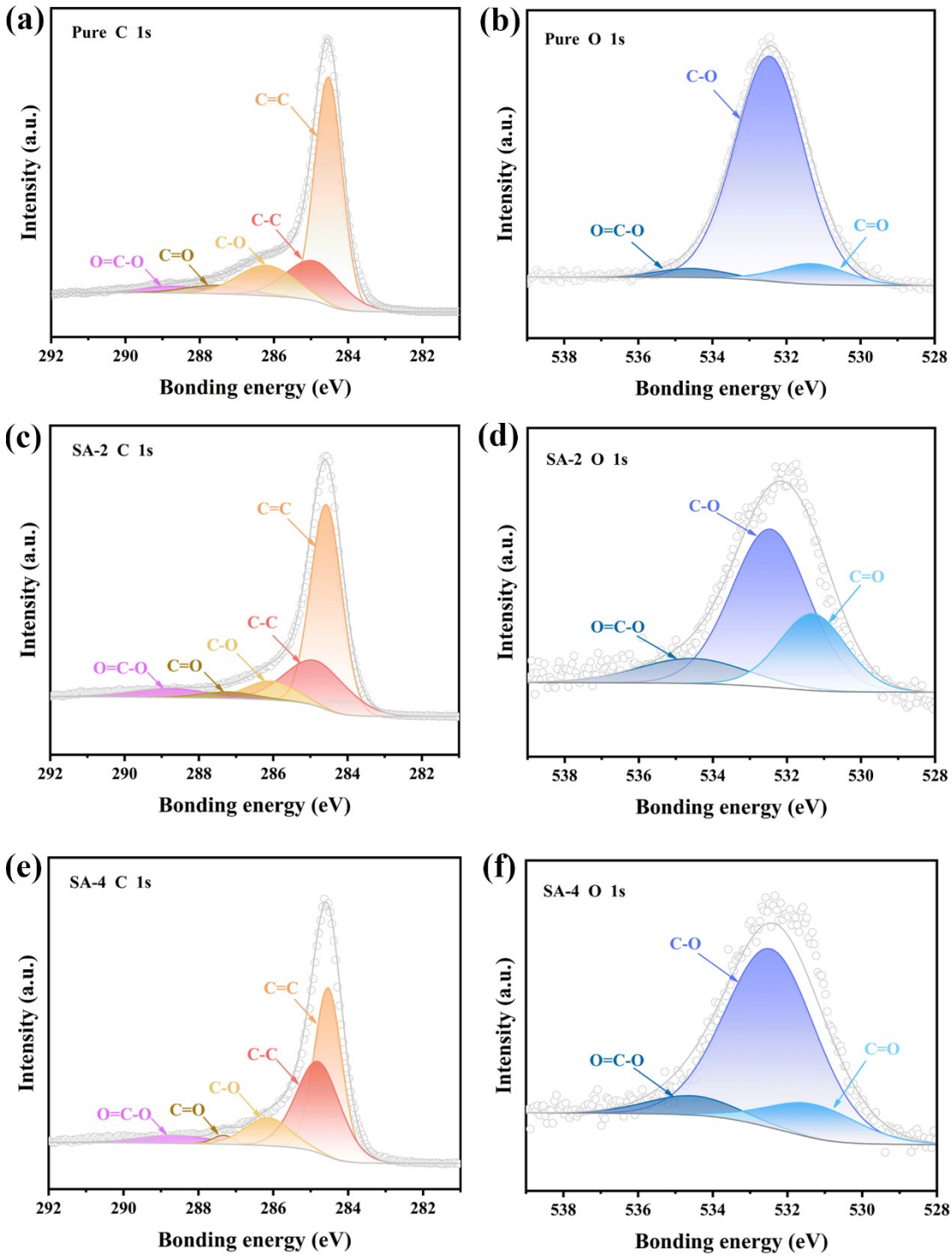

Figure S4 XPS high-resolution spectra of C 1s and O 1s for (a, b) Pure, (c, d) SA-2, (e, f) SA-4.

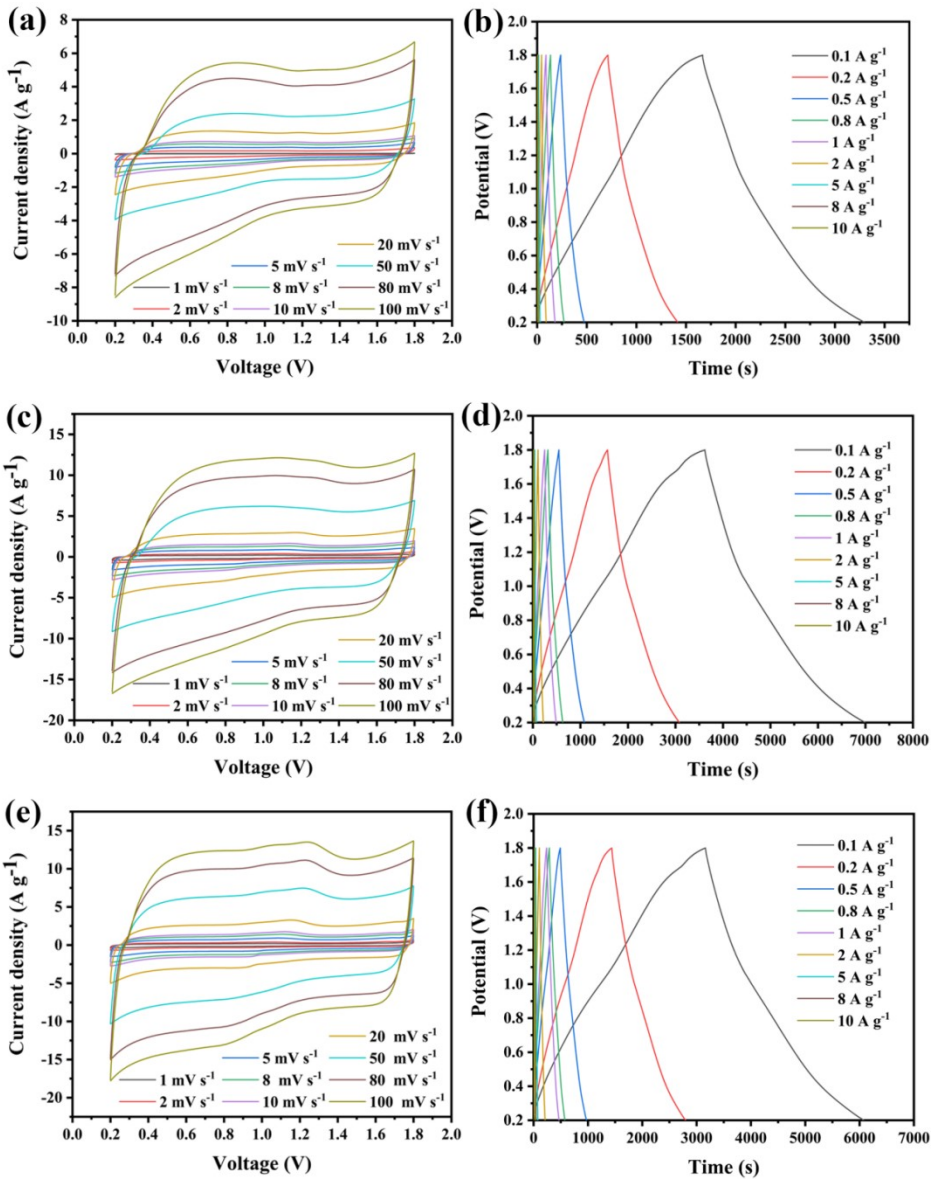

Figure S5 CV curves and GCD plots of (a, b) Pure, (c, d) SA-2, (e, f) SA-4.

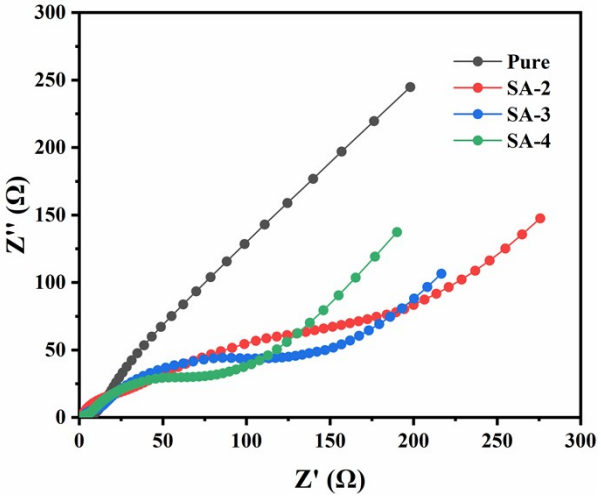

Figure S6 EIS plots of different samples.

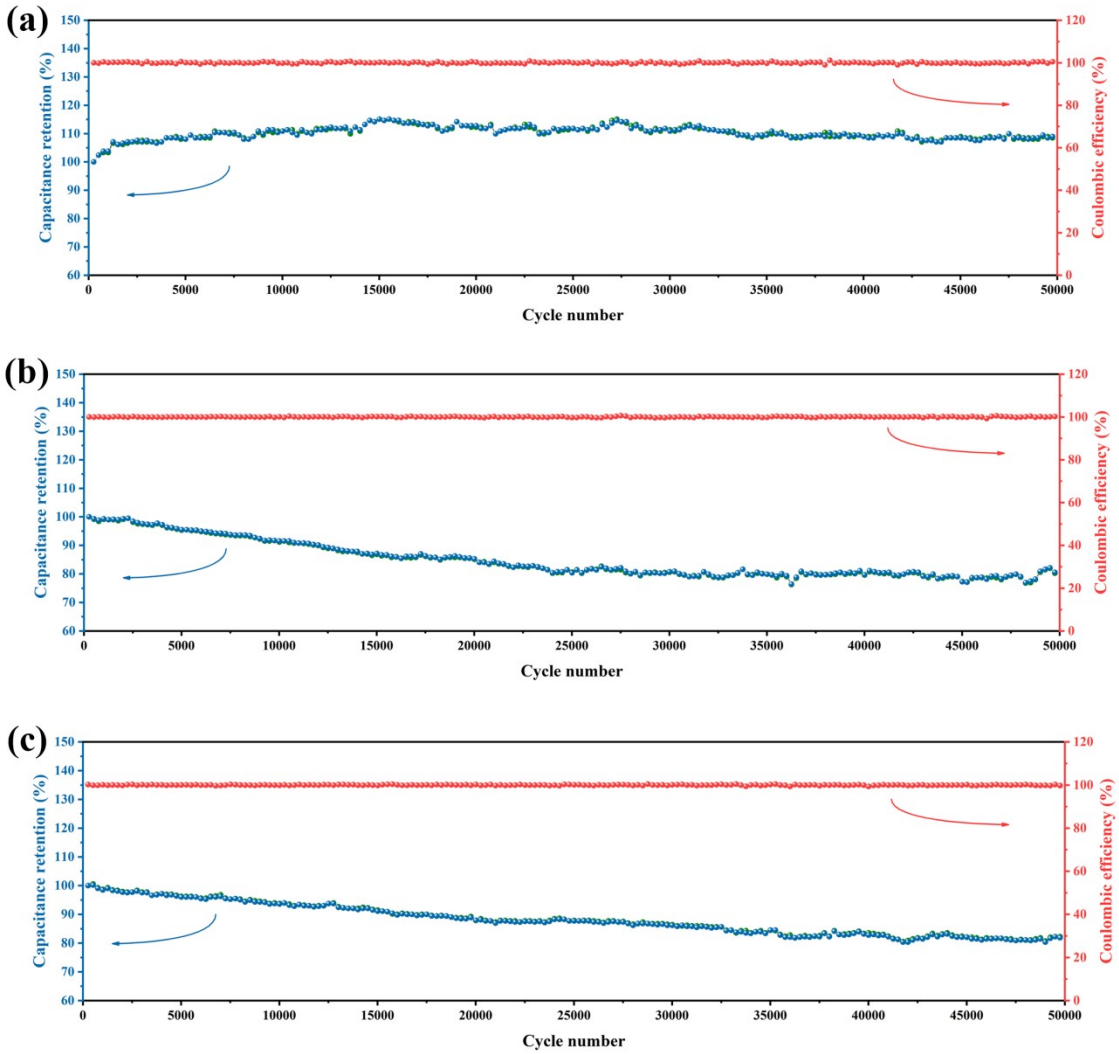

Figure S7 circling performance for ZIHCs based on (a) Pure, (b) SA-2, (c) SA-4 at 5A g^{-1}.

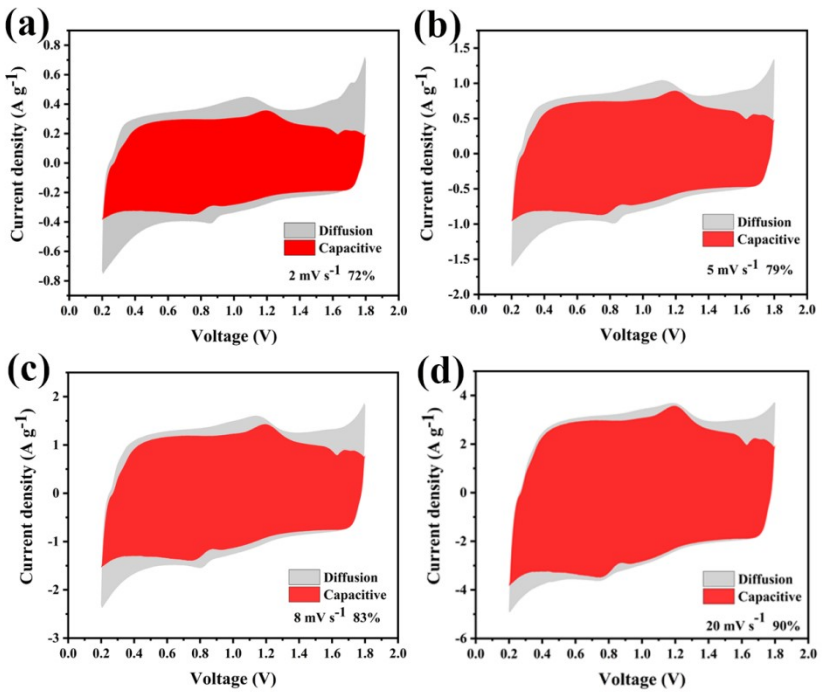

Figure S8 the capacitive contribution at different scan rates of SA-3.

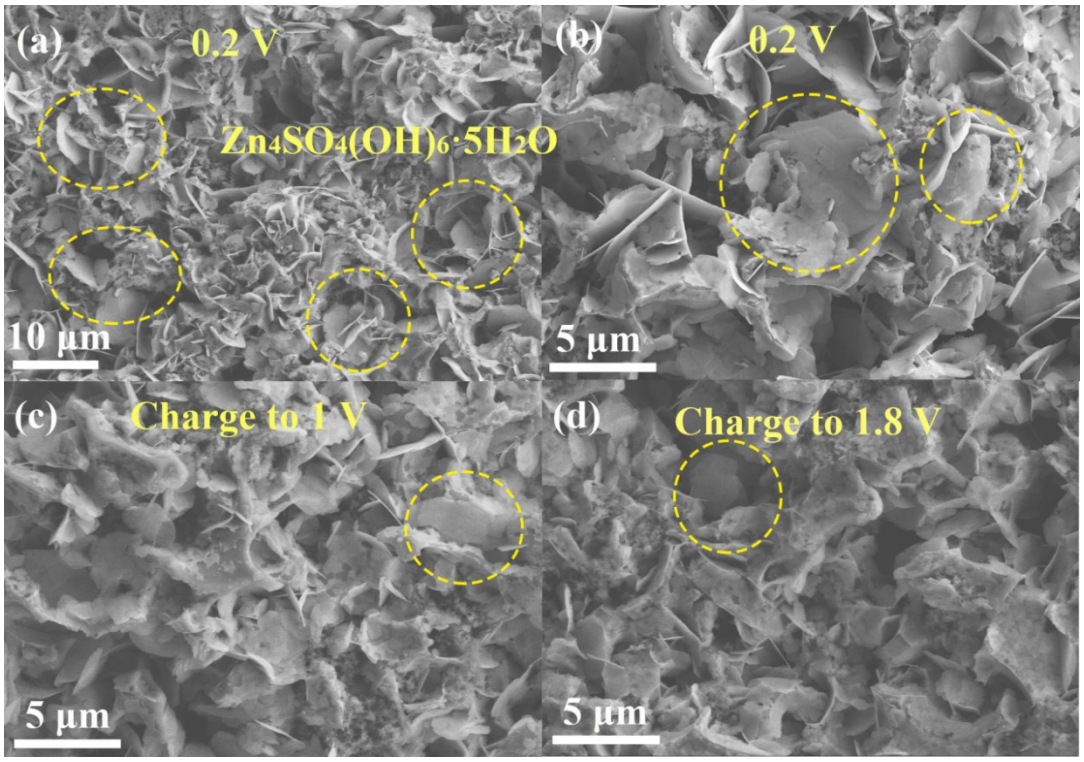

Figure S9 SEM of SA-3 (a) and (b) 0.2V, (c) charge to 1 V, (d) charge to 1.8 V

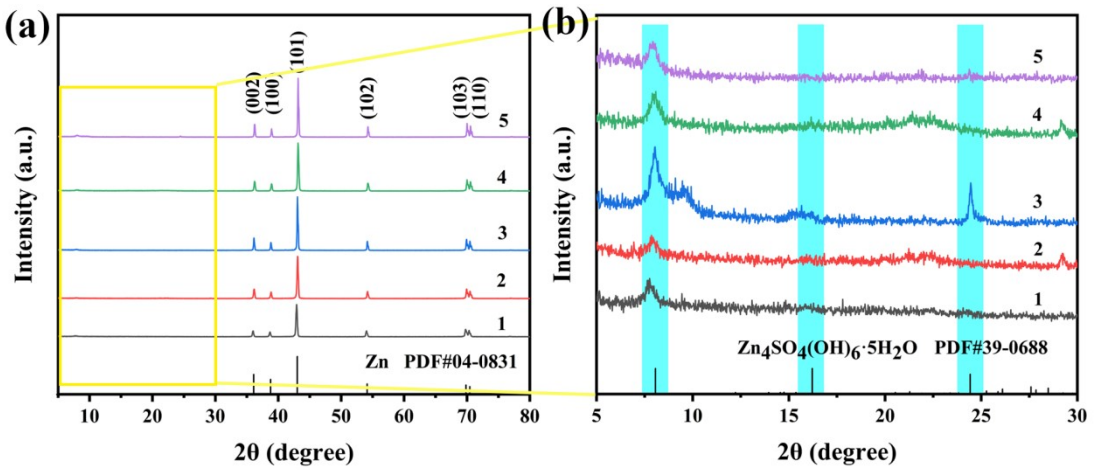
(a)
(b)
Intensity (a.u.)
(002)
(100)
(101)
(102)
(103)
(110)
5
4
3
2
1
Zn PDF#04-0831
2θ (degree)
Zn4SO4(OH)6·5H2O PDF#39-0688

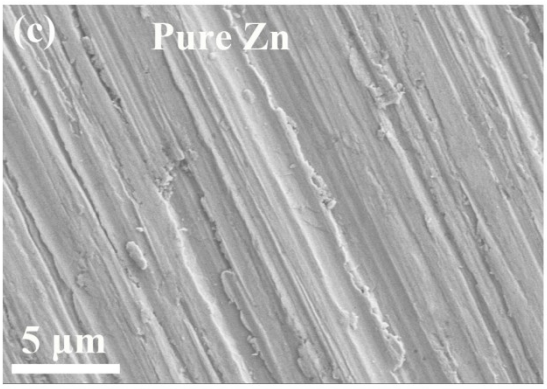
(c)
Pure Zn
5 μm

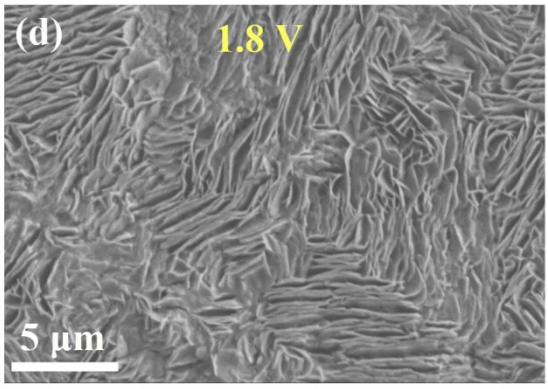
(d)
1.8 V
5 μm

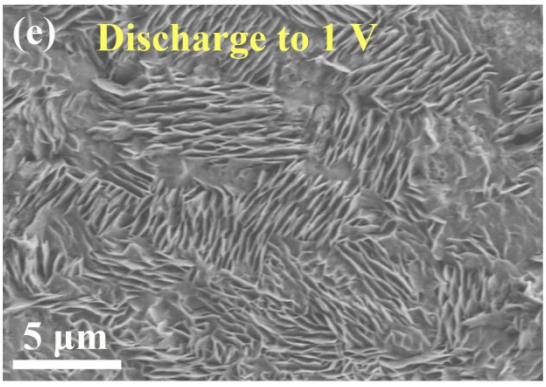
(e)
Discharge to 1 V
5 μm

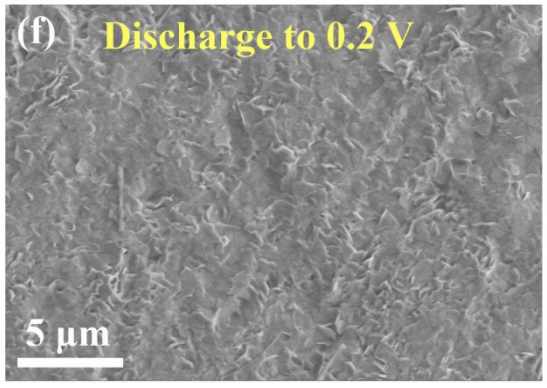
(f)
Discharge to 0.2 V
5 μm

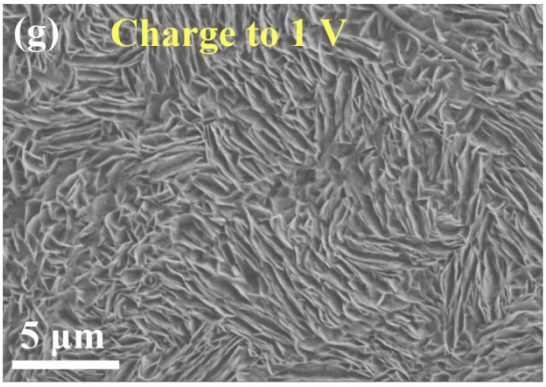
(g)
Charge to 1 V
5 μm

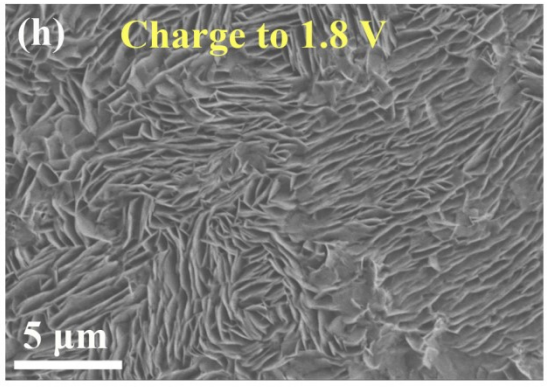
(h)
Charge to 1.8 V
5 μm

Figure S10 (a) the ex situ XRD pattern for corresponding potential of Zn anode, (b) enlarged view for b) ranging from 5° to 30°. SEM image for (c) pure Zn, (d) 1.8 V, (e) discharging to 1 V, (f) discharging to 0.2 V, (g) charging to 1 V, (h) charging to 1.8 V of Zn anode.

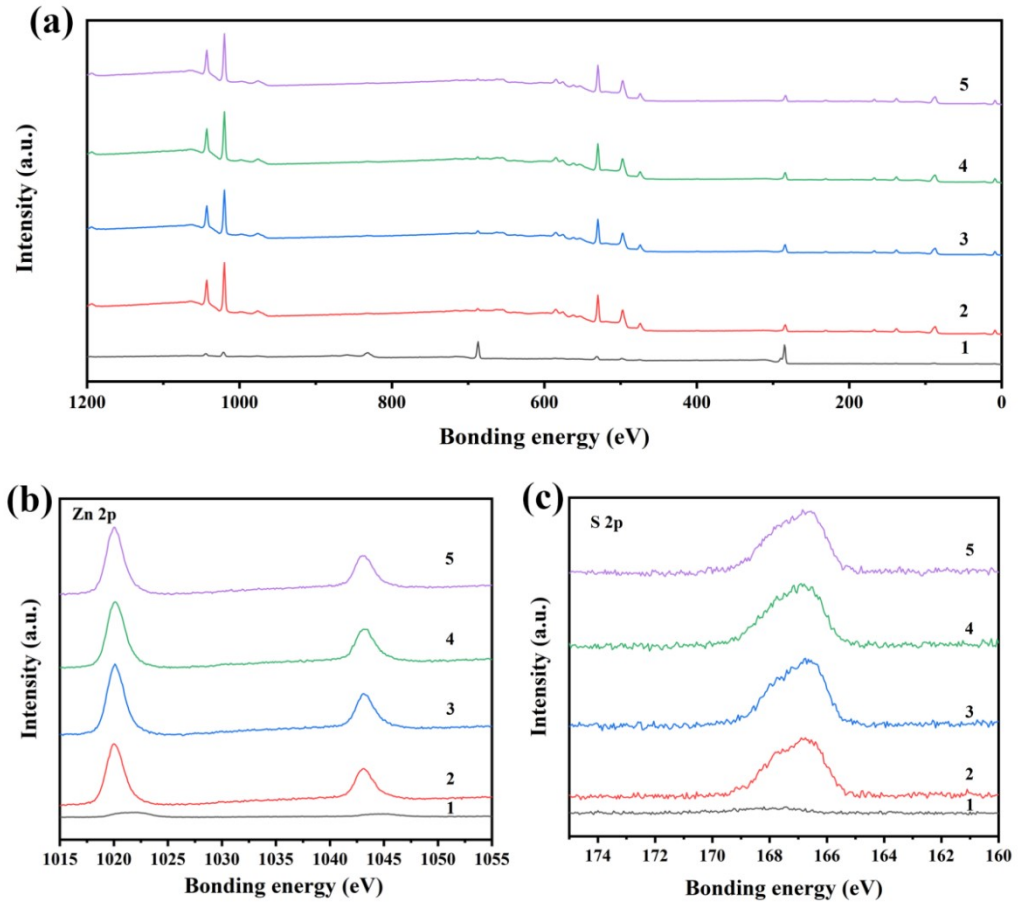

Figure S11 (a) XPS spectrum, XPS spectrum for (b) Zn 2p and (c) S 2p

Table S1 Structural parameters of Pure and SA-x samples

Sample	$S_{BET}/m^2\ g^{-1}$	$S_{micro}/m^2\ g^{-1}$	$V_{total}/cm^3\ g^{-1}$	$V_{micro}/cm^3\ g^{-1}$
Pure	883	329	0.28	0.16
SA-2	1216	475	0.45	0.21
SA-3	1321	456	0.46	0.21
SA-4	1266	237	0.45	0.13

Table S2 C, O ratio of SA-x samples

	C (%)					**O (%)**		
	C=C	C-C	C-O	C=O	O=C-O	C=O	C-O	O=C-O
Pure	55.98	20.08	15.64	4.67	3.63	8.09	88.41	3.50
SA-2	57.03	24.92	8.50	3.24	6.33	25.68	60.83	13.49
SA-3	51.63	28.96	9.54	2.31	7.56	19.24	73.25	7.51
SA-4	43.22	37.71	11.92	1.76	5.38	14.58	77.11	8.31

Table S3 Performance comparison of our ZIHC with reported ZIHCs.

ZIHCs	Energy/Power density	Potential window	Cycle stability
Zn// 1 M $ZnSO_4$// ASICKOH[1]	92 W h kg^{-1}/ 99.5 W kg^{-1} 43 W h kg^{-1}/1.03 kW kg^{-1}	0.1-1.45 V	--
Zn// 1 M $Zn(CF_3SO_3)_2$// AC[2]	61.6 W h kg^{-1}/72 W kg^{-1} 52.7 W h kg^{-1}/1.73 kW kg^{-1}	0-1.8 V	20,000 cycles/ 91%/ 1 A g^{-1}
Zn// 1 M $ZnSO_4$// L-NS-CNS[3]	91 W h kg^{-1}/94 W kg^{-1} 33.8 W h kg^{-1}/9.9 kW kg^{-1}	0.2-1.8 V	18000 cycles/ 94.2%/ 2 A g^{-1}
Zn// 1 M $ZnSO_4$// PCNF-4[4]	142.2 W h kg^{-1}/400.3 W kg^{-1} 68.4 W h kg^{-1}/15.39 kW kg^{-1}	0.1-1.7 V	10000 cycle/ 90%/ 10 A g^{-1}
Zn// 2 M $ZnSO_4$// MCHSs[5]	129.3 W h kg^{-1}/266.4 W kg^{-1} 36.8 W h kg^{-1}/13.7 kW kg^{-1}	0.2-1.8 V	10000 cycle/ 96%/ 1 A g^{-1}
Zn// 2 M $ZnSO_4$// PH-4[6]	117.5 W h kg^{-1}/890 W kg^{-1}	0.1-1.8 V	

	60.7 W h kg^{-1}/16.2 kW kg^{-1}		
This work	**100 W h kg^{-1}/100 W kg^{-1}** **58 W h kg^{-1}/9.9 kW kg^{-1}**	**0.2-1.8 V**	**50000 cycle/ 93%/ 5 A g^{-1}**

1. Naik, P. B.; Yadav, P.; Nagaraj, R.; Puttaswamy, R.; Beere, H. K.; Maiti, U. N.; Mondal, C.; Kotrappanavar, N. S.; Ghosh, D., Developing High-Performance Flexible Zinc Ion Capacitors from Agricultural Waste-Derived Carbon Sheets. *Acs Sustainable Chemistry & Engineering* **2022,** *10* (4), 1471-1481.http://dx.doi.org/10.1021/acssuschemeng.1c06569

2. Wang, H.; Wang, M.; Tang, Y., A novel zinc-ion hybrid supercapacitor for long-life and low-cost energy storage applications. *Energy Storage Materials* **2018,** *13*, 1-7.http://dx.doi.org/10.1016/j.ensm.2017.12.022

3. Jian, W.; Zhang, W.; Wei, X.; Wu, B.; Liang, W.; Wu, Y.; Yin, J.; Lu, K.; Chen, Y.; Alshareef, H. N.; Qiu, X., Engineering Pore Nanostructure of Carbon Cathodes for Zinc Ion Hybrid Supercapacitors. *Advanced Functional Materials* **2022,** *32* (49).http://dx.doi.org/10.1002/adfm.202209914

4. Pan, Z.; Lu, Z.; Xu, L.; Wang, D., A robust 2D porous carbon nanoflake cathode for high energy-power density Zn-ion hybrid supercapacitor applications. *Applied Surface Science* **2020,** *510*.http://dx.doi.org/10.1016/j.apsusc.2020.145384

5. Liu, P.; Liu, W.; Huang, Y.; Li, P.; Yan, J.; Liu, K., Mesoporous hollow carbon spheres boosted, integrated high performance aqueous Zn-Ion energy storage.

Energy Storage Materials **2020,** *25*, 858-865.http://dx.doi.org/10.1016/j.ensm.2019.09.004

6. Fan, H.; Zhou, S.; Li, Q.; Gao, G.; Wang, Y.; He, F.; Hu, G.; Hu, X., Hydrogen-bonded frameworks crystals-assisted synthesis of flower-like carbon materials with penetrable meso/macropores from heavy fraction of bio-oil for Zn-ion hybrid supercapacitors. *Journal of Colloid and Interface Science* **2021,** *600*, 681-690.http://dx.doi.org/10.1016/j.jcis.2021.05.042